Journal of Hydrology 464–465 (2012) 363–375

Contents lists available at SciVerse ScienceDirect

Journal of Hydrology

journal homepage: www.elsevier.com/locate/jhydrol

Estimating river bathymetry from data assimilation of synthetic SWOT measurements

Yeosang Yoon [a,c,*], Michael Durand [b,c], Carolyn J. Merry [a,c], Elizabeth A. Clark [d], Konstantinos M. Andreadis [e], Douglas E. Alsdorf [b,c]

[a] Department of Civil, Environmental, and Geodetic Engineering, The Ohio State University, Columbus, OH 43210, USA
[b] School of Earth Sciences, The Ohio State University, Columbus, OH 43210, USA
[c] Byrd Polar Research Center, The Ohio State University, Columbus, OH 43210, USA
[d] Department of Civil and Environmental Engineering, University of Washington, Seattle, WA 98195, USA
[e] Jet Propulsion Laboratory, California Institute of Technology, Pasadena, CA 91109, USA

ARTICLE INFO

Article history:
Received 7 November 2011
Received in revised form 8 June 2012
Accepted 15 July 2012
Available online 24 July 2012
This manuscript was handled by Konstantine P. Georgakakos, Editor-in-Chief, with the assistance of Ioannis K Tsanis, Associate Editor

Keywords:
SWOT
Hydrologic/hydraulic modeling
Data assimilation
Ensemble Kalman Filter
River bathymetry
River discharge

SUMMARY

This paper focuses on estimating river bathymetry for retrieving river discharge from the upcoming Surface Water and Ocean Topography (SWOT) satellite mission using a data assimilation algorithm coupled with a hydrodynamic model. The SWOT observations will include water surface elevation (WSE), its spatial and temporal derivatives, and inundated area. We assimilated synthetic SWOT observations into the LISFLOOD-FP hydrodynamic model using a local ensemble batch smoother (LEnBS), simultaneously estimating river bathymetry and flow depth. SWOT observations were obtained by sampling a "true" LISFLOOD-FP simulation based on the SWOT instrument design; the "true" discharge boundary condition was derived from USGS gages. The first-guess discharge boundary conditions were produced by the Variable Infiltration Capacity model, with discharge uncertainty controlled via precipitation uncertainty. First-guess estimates of bathymetry were derived from SWOT observations assuming a uniform spatial depth; bathymetric variability was modeled using an exponential correlation function. Thus, discharge and bathymetry errors were modeled realistically. The LEnBS recovered the bathymetry from SWOT observations with 0.52 m reach-average root mean square error (RMSE), which was 67.8% less than the first-guess RMSE. The RMSE of bathymetry estimates decreased sequentially as more SWOT observations were used in the estimate; we illustrate sequential processing of 6 months of SWOT observations. The better estimates of bathymetry lead to improved discharge estimates. The normalized RMSE of the river discharge estimates was 10.5%, 71.2% less than the first-guess error.

© 2012 Elsevier B.V. All rights reserved.

1. Introduction

Satellite remote sensing data has been used to estimate river discharge, complementing data measured by existing in situ gage networks. River discharge, however, cannot be directly measured from space; thus observable hydraulic data, such as channel width, water surface elevation (WSE), slope, and cross-sectional area, have been used to estimate discharge (e.g., Alsdorf et al., 2007a; Bjerklie et al., 2005; Brackenridge et al., 2005; Kouraev et al., 2004; LeFavour and Alsdorf, 2005).

The upcoming Surface Water and Ocean Topography (SWOT) mission will directly provide simultaneous mapping of inundation area and inland WSE (i.e., river, lakes, wetlands, and reservoirs), both temporally and spatially, using a Ka-band radar interferometer (Alsdorf et al., 2007a; Durand et al., 2010b); this mission is planned to launch in 2019. In addition, based on the dynamic water mask from SWOT, the channel centerline and widths can be extracted, following Pavelsky and Smith (2008). With these observations, the SWOT mission will provide measurements of water storage changes in terrestrial surface water bodies (Lee et al., 2010) and information for characterizing river discharge at global scales for all rivers 100 m and wider and perhaps as narrow as 50 m in width (Rodríguez, 2009). Using existing technology, it is possible to indirectly estimate WSE by the spatial intersection of a water mask and a digital terrain model (DTM). For example, the combination of all-weather Synthetic Aperture Radar (SAR) inundation extent and a DTM is useful in estimation of WSE for flood monitoring (e.g., Hostache et al., 2009; Schumann et al., 2010;

* Corresponding author. Present address: The Ohio State University, 470 Hitchcock Hall, 2070 Neil Ave., Columbus, OH 43210, USA. Tel.: +1 6145604817; fax: +1 6142923780.

E-mail addresses: yoon.203@osu.edu (Y. Yoon), durand.8@osu.edu (M. Durand), merry.1@osu.edu (C.J. Merry), eclark@hydro.washington.edu (E.A. Clark), konstantinos.m.andreadis@jpl.nasa.gov (K.M. Andreadis), alsdorf.1@osu.edu (D.E. Alsdorf).

0022-1694/$ - see front matter © 2012 Elsevier B.V. All rights reserved.
http://dx.doi.org/10.1016/j.jhydrol.2012.07.028

Zwenzner and Voigt, 2009). However, as Alsdorf et al. (2007b) have shown, such shoreline methods do not characterize WSE for complex floodplain geomorphologies, such as those of the Amazon. In contrast, SWOT will directly measure WSE; see Alsdorf et al. (2007a) for a comprehensive review of existing technologies and methods.

Because SWOT will measure WSE, not the true depth to the river bottom, the cross-sectional flow area will not be fully measured. The SWOT sensor can directly measure the changes in water depth and cross-sectional area above the lowest measured WSE, but absolute river depths will not be observed. Once obtained, an estimate of bathymetry would provide the remaining information needed to estimate true cross-sectional flow area and river depth, thus improving discharge estimation from SWOT measurements. Some studies have shown the potential to estimate coastal and stream bathymetry from optical sensors based on the relationship between water depth and spectral reflectance (e.g., Lafon et al., 2002; Fonstad and Marcus, 2005; Zhang et al., 2011); however, this method works only for shallow waters with little or no sediment load.

Data assimilation can be used to extract information, such as bathymetry, that is not directly observable from the spaceborne measurements (Reichle, 2008). Recent research has shown the potential of SAR-derived WSE to reduce the uncertainty of a hydraulic model, using data assimilation techniques, to support flood monitoring (e.g., Giustarini et al., 2011; Matgen et al., 2010; Neal et al., 2009). However, these methods only apply to high flow conditions (i.e., out-of-bank flood event) at local scales with a high resolution DTM (i.e., derived from a Light Detection and Ranging (LiDAR) sensor). Data assimilation schemes have also been used to characterize discharge from simulated SWOT measurements. Andreadis et al. (2007) estimated river flow depth and discharge using an assimilation scheme of WSE data, which were simulated by the LISFLOOD-FP (Bates and De Roo, 2000; Trigg et al., 2009) model with boundary inflows from the Variable Infiltration Capacity (VIC) model (Liang et al., 1996). They showed that the Ensemble Kalman Filter (EnKF) can reduce the river discharge root mean square error (RMSE) from 23.2% to 10% over an 84-day simulation period compared to the estimate without assimilation; river bathymetry was assumed to be known. Durand et al. (2008) demonstrated an ensemble-based data assimilation method for estimating bathymetric depths and slopes from WSE measurements and the LISFLOOD-FP model over a 240-km reach of the Amazon River floodplain. Their scheme was able to recover the bathymetric depth and slope to within 56 cm and 0.30 cm/km, respectively, by exploiting the flooding extent over the Amazon River floodplain. However, their results were limited by the assumption of simplified bathymetry; spatial variations in bathymetry at scales finer than 50 km were not modeled. Biancamaria et al. (2011) assimilated synthetic SWOT observations of the Ob River to estimate river water depth variations, with river bathymetry assumed to be known. They showed that the assimilation scheme at the nominal orbit of the mission reduced the spatial and temporal RMSE of the water depth by 59% and 66%, respectively. These studies either neglected bathymetry error, or treated bathymetry in a simplified way, which does not represent realistic spatial variations of bathymetry.

The goal of this study is to find an optimal way to estimate bathymetry in order to reduce the uncertainty in SWOT estimates of discharge in a large river system. Here, we introduce a new assimilation approach as an extension of the EnKF to estimate bathymetry from observed WSE coupled with a hydrodynamic model. We assume that hydrodynamic model simulations of large rivers are largely governed by discharge boundary conditions, bathymetry, and roughness coefficients (Manning's n). The Manning's n may be defined on the basis of the physical characteristics of the river (Chow, 1959); nonetheless, such a priori estimates will have some associated uncertainty. While a data assimilation scheme could provide estimates of both the roughness coefficient and bathymetry, uncertainty in the Manning's n is not considered in this study due to the focus on the bathymetry uncertainty; future work will address the roughness coefficient. Realistic modeling of errors in boundary inflows and bathymetry is critical for evaluating discharge estimates derived from SWOT measurements. In this study, the true discharge boundary conditions come from USGS streamflow gages, rather than a model. The first-guess discharge boundary condition is derived from the VIC hydrologic model (Liang et al., 1994) driven by meteorological data (Maurer et al., 2002) that is similar to what is globally available. First-guess estimates of bathymetry are derived from measured SWOT heights assuming a spatially uniform depth with spatially correlated downstream variability. Having realistically described uncertainties in discharge and bathymetry, we evaluate the ability of a data assimilation algorithm to recover bathymetry and discharge using SWOT observations.

2. Description of the study area

Our study area is the Ohio River Basin; the Ohio River flows from Pittsburgh, PA to the Mississippi River at Cairo, IL (Fig. 1). The river is approximately 1580 km long and drains an area of 528,000 km^2. The annual average flow is 8733 m^3/s, which is the third largest river by discharge in the United States (Benke and Cushing, 2005). We chose 12 of the major Ohio River tributaries and seven of the minor Ohio River tributaries to include in the hydrodynamic model; the 12 major and seven minor tributaries represent a total of 474211 km^2 (89.8%) of the Ohio River Basin drainage area (for details, see Table 1). The remaining 10.2% of the drainage area is drained by minor streams, which we do not model explicitly in this study.

3. River model

We use an observing system simulation experiment (OSSE; e.g., Andreadis et al., 2007) to assess the potential capabilities of the assimilation system to characterize river bathymetry. The OSSE largely consists of two separate simulations; the first is the "true" simulation, which is used to generate synthetic SWOT observations over the entire Ohio River and to evaluate the assimilation results. The second simulation is the "open-loop" simulation, which is forced using corrupted model inputs, namely discharge boundary conditions and river bathymetry.

The LISFLOOD-FP hydrodynamic model (Bates and De Roo, 2000; Trigg et al., 2009) was used to generate both the "truth" and "corrupted" estimates for the assimilation. The model uses a two-dimensional (2-D) diffusion wave representation of floodplain flow and a one-dimensional (1-D) approach to simulate river channel flow using a rectangular channel geometry assumption. Here, we utilized the 1-D scheme to develop an algorithm for in-channel flow based on the diffusive wave approximation to the full St. Venant equations (Trigg et al., 2009). To model the Ohio River in the LISLOOD-FP model, estimates of the river centerline, channel bed elevation along the centerline, and channel width are needed, as well as the boundary inflow data for each tributary. The "true" and the "open-loop" discharge boundary conditions and river bathymetry are derived from completely different datasets.

3.1. True simulation

The river centerlines, including those of the major tributaries were manually defined at an approximately 500-m spatial resolu-

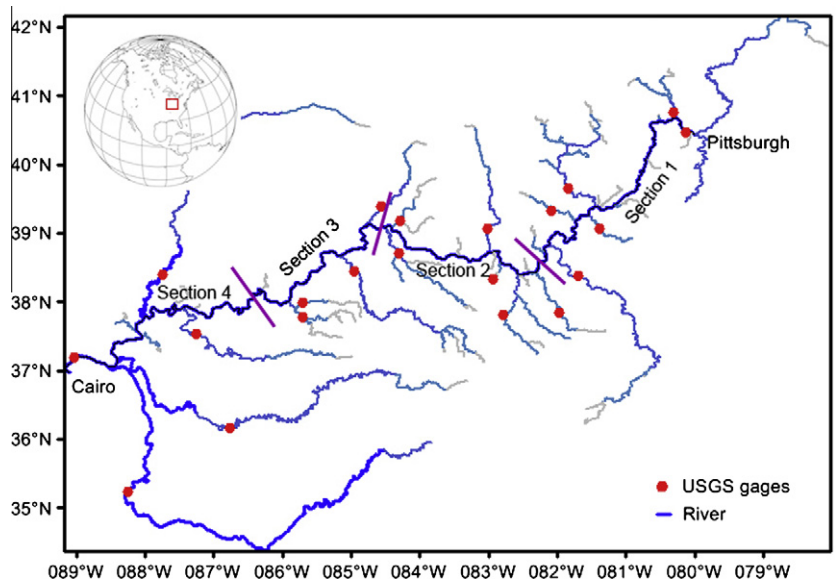

Fig. 1. A map of the Ohio River, including 12 major tributaries and seven minor tributaries used in the model. The contributing drainage area of each tributary is shown by the relative thickness of the blue lines. The USGS gages (red dots) used for the boundary conditions are shown. Solid lines divide the river into four sections that were used for the analysis of results.

Table 1
Drainage area of each of the 12 major (bold tributary name) and seven minor tributaries included in the model.

Tributary name	Flow distance from upstream (km)	Drainage area (km^2)	USGS gauge ID	Drainage area at gage (km^2)	Drainage area covered by gauge (%)
Beaver River	20.3	8106.7	03107500	8044.5	99.2
Muskingum River	250.5	20823.5	03150000	19222.9	92.3
Little Kanawha River	269.2	6008.8	03155000	3926.4	65.3
Hocking River	291.9	3082.1	03159500	2442.4	79.2
Kanawha River	396.2	31597.9	03198000	27060.2	85.6
Guyandotte River	447.0	4325.3	03203600	2157.5	49.9
Big Sandy River	457.9	11085.1	03212500	5552.9	50.1
Little Sandy River	508.9	1875.2	03216500	1036.0	55.2
Scioto River	540.3	16860.8	03237020	15115.2	89.6
Little Miami River	710.4	4325.3	03245500	3115.8	72.0
Licking River	720.4	9505.3	03253500	8547.0	89.9
Great Miami River	754.7	13985.9	03274000	9401.7	67.2
Kentucky River	838.2	18052.2	03290500	16006.1	88.7
Salt River	972.3	7485.1	03298500	3100.2	41.4
Green River	1213.8	23905.6	03320000	19595.9	82.0
Wabash River	1313.3	85728.6	03377500	74164.3	86.5
Cumberland River	1431.2	46412.6	034315005	33307.2	71.8
Tennessee River	1449.5	105956.4	03593500	85832.2	81.0
Sum		**474211.3**[a]		**392717.3**[a]	82.8
Ohio River Basin		528202.18[b]			

[a] The area includes the upstream drainage area (Allegheny and Monongahela River) on the mainstream of the Ohio River.
[b] The area includes all the additional smaller tributaries that drain into the Ohio River.

tion, combining data from the U.S. Army Corps of Engineers (USACE) dataset, which is a point layer at a spatial resolution of 8 km, with the data from the HydroSHEDS (USGS HydroSHEDS, http://hydrosheds.cr.usgs.gov) river network, derived from the Shuttle Radar Topography Mission at a 15 arc-sec resolution. To make the true model as realistic as possible, channel bed elevation, width, and roughness were extracted from the USACE dataset. (Note that the USACE true bathymetric data were not used for the open-loop simulation.) The USACE dataset was developed for the CASCADE model (for details, see Lee et al., 2003), which is an operational model of the Ohio River system. Note that the low (8 km) spatial resolution of the CASCADE model is not appropriate to generate synthetic SWOT observations for use in this study; thus we used the LISFLOOD-FP model in this study. The LISFLOOD-FP model uses the rectangular channel assumption for river flow modeling; thus, bed elevation, effective channel width and roughness coefficients were extracted along the Ohio River from the USACE dataset. The CASCADE model represents the river cross-sectional flow area A as a function of river stage or height h. The rectangular approximation to this stage-area curve is given by A_s, which is calculated from the best-fit line to the true $A(h)$ curve over the range of h modeled over a 1-year simulation:

$$A_s(h) = a_1 h + a_0 \tag{1}$$

Here a_1 is the effective river width; h is the water elevation; and a_0 is an offset parameter. The bed elevation can be found by setting $A(h) = 0$, and solving for h, the elevation corresponding to the zero cross-sectional area; the effective bed elevation is thus equal to $-a_0/a_1$.

The boundary inflow of the 12 major and seven minor tributaries was obtained from the USGS streamflow gage network from March 1, 1996 to August 24, 1996 (176 days). Also, the outlet stage from the USGS gage (03611500) was used as the downstream boundary condition, following previous work (e.g., Andreadis et al., 2007; Durand et al., 2010a). Note that the first-guess boundary inflows were obtained independently from the gage measurements using the VIC model, and their development is described in more detail in Section 3.2.2. Fig. 1 shows the location of each gage used as a boundary condition; detailed information for each gage is shown in Table 1. The gages represent between 50% and 99% of the total drainage area of each tributary. Taken together, the gages represent a total of 392,717 km^2, which is approximately 74.3% of the Ohio River Basin drainage area. To make the model as realistic as possible, compensation for the remaining 25.7% of the drainage area is needed. To accomplish this, we scaled the discharge based on the 30-year (1979–2008) average discharge and drainage area of each tributary, by assuming a power law relationship (Furey and Gupta, 2005) between the mean discharge Q_{gage} and drainage area B_{gage} at the gage; defined as:

$$Q_{gage} = bB_{gage}^{c} \tag{2}$$

where b and c are best-fit coefficients. Then we estimated the total flow Q_{tot} by scaling Q_{gage} by the ratio of B_{gage} to B_{tot}:

$$Q_{tot} = Q_{gage}\left(\frac{B_{tot}}{B_{gage}}\right)^{c} \tag{3}$$

To verify that this LISFLOOD-FP model setup, used to generate the true discharge and synthetic SWOT observations, is producing reasonable results, we compared the simulated discharge at the modeled basin outlet on the Ohio River with the observed discharge at the USGS gage at the same location. Although the stage used for the model boundary condition and the model-calculated discharge are highly dependent, this comparison is intended to show that the model is producing reasonable results. Fig. 2a shows estimates of river discharge at the downstream model outlet. The model discharge matches the observed discharge with a normalized root mean square error (NRMSE) of 27.0% and a correlation coefficient of 0.93. The LISFLOOD-FP model does not perfectly represent the real system; for instance, the navigation locks and dams on the Ohio River were not modeled (Lee et al., 2003). In addition, model performance might improve if we were to use a downstream height boundary condition that is located further downstream than where we are evaluating the discharge, in order to avoid any backwater effect. Still, we attempted to simulate the real system closely based on the given ancillary data from the USACE and gage dataset using the up-scaling scheme. Note that since the model was used to generate synthetic data for the assimilation, the accuracy of the model is not the major issue for this study; thus no LISFLOOD-FP model calibration was performed. Fig 2b shows examples of modeled WSE on August 24, 1996 and the bathymetry along the Ohio River. WSE from the true simulation were used to simulate the synthetic SWOT observations, as described in Section 4. The spatial resolution of the LISFLOOD-FP model at the 500-m resolution indicates significant spatial variations in the bathymetry, e.g., adverse bed slopes over short distances are not uncommon.

3.2. Open-loop simulation for ensemble member generation

Data assimilation schemes combine observations with forecast model states in order to obtain 'the best' estimate of the current model states. The open-loop simulation was used to simulate ensemble and ensemble covariance of forecast model states. The open-loop ensemble is generated by: (1) creating an ensemble of hydrodynamic model inputs of bathymetry and boundary inflows, and (2) propagating the ensemble of model inputs through the model.

According to Evensen (2009), as the size n of the ensemble increases, the errors in the Monte Carlo sampling decrease with $1/\sqrt{n}$. The size of the ensemble, however, highly affects the computational cost of the data assimilation. A bigger problem is that the LISFLOOD-FP model, used to generate ensembles, requires significantly higher computational cost than the data assimilation algorithm based on the given assumptions (Hunter et al., 2008; Neal et al., 2011); thus, we limited the ensemble size to 20 members of bathymetry and boundary inflows of each tributary, respectively, for the algorithm, following previous work (e.g., Andreadis et al., 2007; Biancamaria et al., 2011; Durand et al., 2008).

Manning's n is one of the crucial components for the model; however, it may be incorporated in the hydraulic model following a simplified assumption. For example, Andreadis et al. (2007) and Neal et al. (2009) used a spatially uniform Manning's n selected based on the characteristics of the natural river type (e.g., for details, see Chow, 1959). Giustarini et al. (2011) used the Manning's n calibrated by using rating curves; however, this approach requires gaging data to calibrate the coefficients, which prohibits its use in ungaged basins. In this study, we focus on estimation of river bathymetry, and uncertainty in the Manning's n is not considered. Future studies will explore simultaneous estimation of roughness, bathymetry, and flow.

3.2.1. Bed elevation

Creation of a first-guess bathymetry ensemble required two steps. First, an initial bathymetry profile $\tilde{z}$ along the Ohio River was obtained by subtracting a spatially-uniform nominal water depth of 7 m from mean SWOT WSE measurements. Second, the

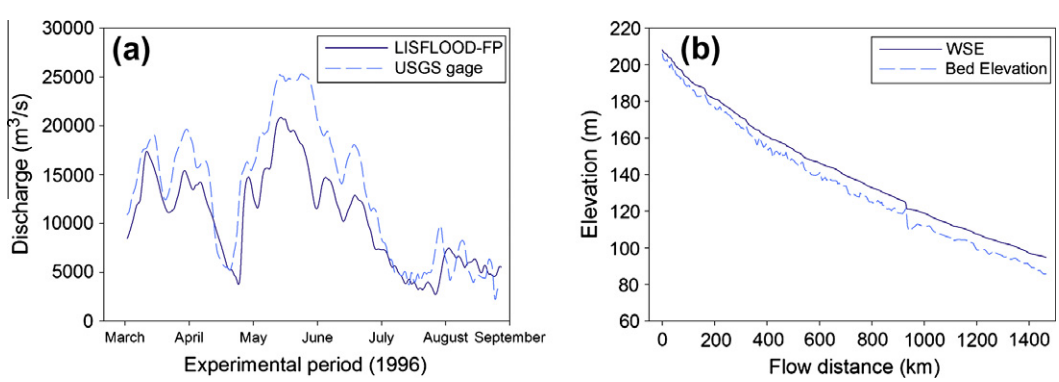

Fig. 2. "True" LISFOOD-FP model results are shown for the Ohio River. (a) Modeled discharge at the downstream model outlet, as well as the discharge from the USGS gage. (b) Example of WSE on August 24, 1996 and the bathymetry.

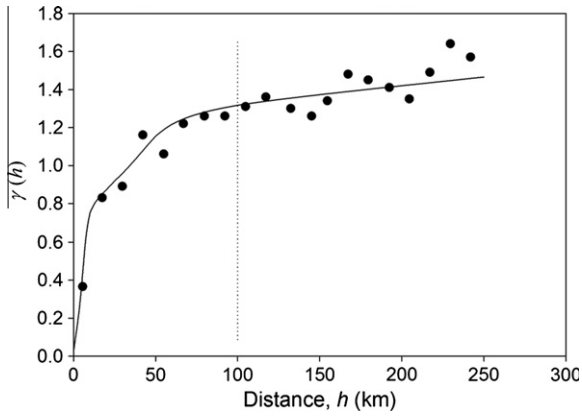

Fig. 3. The semivariogram model for the bed elevation.

bathymetry uncertainty and spatial variability were represented using the covariance matrix C; the covariance matrix was calculated using an exponential model of the bathymetry spatial autocorrelation:

$$C = \sigma^2 \exp^{-\frac{3X}{L}} \tag{4}$$

where X is the vector of distances between the modeled pixels over the entire river. The spatial correlation length L was assumed to be 100 km, estimated by a semivariogram analysis; Fig. 3 shows the semivariogram results. The standard deviation σ was assumed to be 2.5 m. Finally, 20 ensemble members of bathymetry z_k^- were independently generated by adding noise z_{err} to $\tilde{z}$:

$$z_k^- = \tilde{z} + z_{err} \tag{5}$$

where the subscript k denotes ensemble member. The errors z_{err} were represented from the multivariate normal distribution with zero mean and covariance C.

3.2.2. Boundary conditions

Errors in the boundary inflow of each tributary were simulated by corrupting the precipitation inputs to the VIC model (Liang et al., 1994, 1996). VIC is a macroscale hydrologic model that solves surface energy and water balances over a grid cell and has been widely applied to studies of water resources management, land–atmosphere interactions of moisture, and climate change (e.g., Bowling and Lettenmaier, 2010; Maurer et al., 2002). Precipitation used to force macroscale hydrologic models exhibits both spatial and temporal errors (Nijssen and Lettenmaier, 2004; Lowrey and Yang, 2008). Here, corrupted precipitation was modeled by adding storm location errors to the spatial distribution of interpolated in situ observations of precipitation (Maurer et al., 2002). Errors in the latitude and longitude location of the storm center were inferred from differences between daily precipitation fields from the European Centre for Medium-Range Weather Forecasts (ECMWF) 40-year re-analysis data (ERA-40, http://data.ecmwf.int/) and interpolated precipitation data from in situ measurements (Maurer et al., 2002). Initially, the center of mass was calculated for precipitation in the Ohio River Basin from the Maurer et al. (2002) ground-based data set and from ERA-40 for each time step. Then the differences in the center of mass between the two data sets were calculated, and assumed to be representative of the uncertainty of the location of rainfall events. A Gaussian distribution was then fit to the differences, both in terms of latitude and longitude. Finally, 20 ensemble members of precipitation were generated by shifting the entire Maurer et al. (2002) precipitation field at each time step by applying additive latitude errors, with 0.24° mean and a standard deviation of 1.33°, and additive longitudinal errors, with 0.05° mean and a standard deviation of 1.91°. Note that we did not explicitly model uncertainty in the precipitation event magnitude; however, due to the perturbation of the precipitation position, storms often moved in or out of the study area. As a result, uncertainty in precipitation magnitude was implicitly represented in each ensemble member. Because precipitation magnitude errors were not explicitly modeled, the assimilation scheme effectively gives more weight to the coupled VIC and LISFLOOD-FP model (and less weight to the SWOT WSE observations) in the assimilation. It is, therefore, possible that inclusion of precipitation magnitude errors would improve results in this paper. A full assessment of precipitation errors will be taken into account in a future study.

The 20 ensembles of the first-guess downstream boundary condition were generated by adding noise to synthetic SWOT WSE observations, which are described in Section 4. The uncertainty in the downstream boundary condition was modeled by zero mean Gaussian random error with a standard deviation of 0.5 m.

3.2.3. Ensemble generation

Fig. 4 shows examples of the ensemble statistics for the data assimilation scheme, which is a best-case scenario during the experimental period. In most cases, generated ensembles contained significant bias, which is described in more detail in Section 7.2. Fig. 4a shows the discharge of the 20 ensemble members along the main stem of the Ohio River on March 12. The ensemble range does not include the true discharge on most cross-sections due to bias in the boundary inflows. Fig. 4b shows the relative bias of the flow shown in Fig. 4a. The relative bias of flow ε, is determined by:

$$\varepsilon_p = \frac{\left|\bar{Q}_{p,est} - Q_{p,true}\right|}{Q_{p,true}} \tag{6}$$

The upstream inflow, which includes two of the major tributaries, the Allegheny and Monongahela Rivers, has a bias of 26.6%. As flow from each tributary enters the Ohio River, the bias changes. Overall, the bias of the upstream part (flow distance less than 1200 km) shows values larger than 20% and shows a slightly downward trend from upstream to downstream, which means that the underestimated upstream inflow highly affected the entire upstream section, despite better estimates of discharge at other tributaries entering along the upstream section. In addition, after the Green, Wabash, and Cumberland Rivers at locations around 1210, 1310, and 1430 km from the upstream location, respectively, join the Ohio River, the bias sharply decreased. The reason is that the VIC model overestimated the discharge of those rivers. Differences between true and modeled discharge could be caused by both a mismatch between true precipitation and precipitation estimated by Maurer et al. (2002), and errors in the VIC model parameterization and model structure. Fig. 4c and d show ensembles of water depth and bed elevation, respectively, for March 12, 1996.

4. SWOT observations

We generated synthetic SWOT observations for the main stem of the Ohio River using the true simulation described in Section 3.1. The synthetic SWOT observations were generated by using the SWOT swath coverage over the study site, and estimates of water level that were obtained from the LISFLOOD-FP simulation results. The generation of SWOT observations started with obtaining the swath coverage by deriving the ground track. The latter was accomplished using the heading of the satellite with a 22-day revisit time and 78° inclination (Rodríguez, 2009), as well as the predicted satellite locations (latitude and longitude). This track (i.e., the ground location path of the satellite) was used to generate

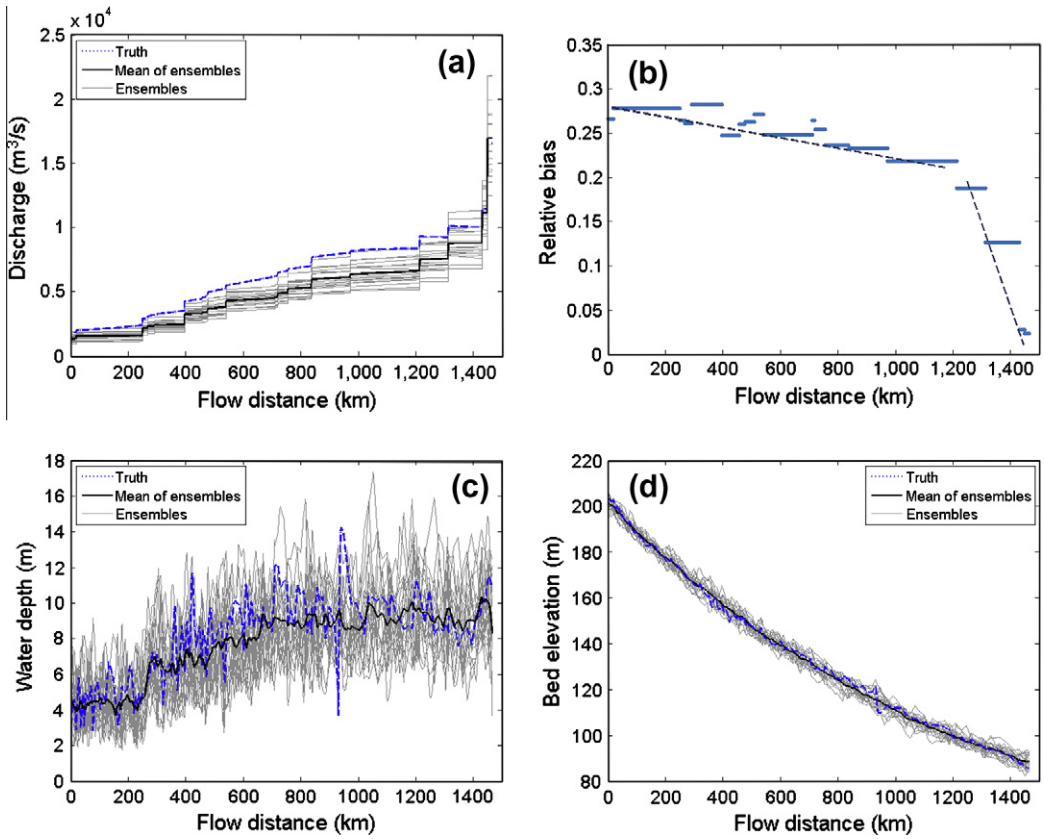

Fig. 4. Examples of the ensemble members for the data assimilation; (a) ensembles of 20 possible discharges along the Ohio River, (b) the relative bias of the flow, (c) ensembles of the water depth, and (d) ensembles of the bed elevation for March 12, 1996 are shown, as well as the mean and simulated truth values.

the SWOT observational swath with a proposed 140-km swath width of the ground path. Fig. 5 shows the SWOT coverage of the Ohio River with the LISFLOOD-FP modeled pixels and the number of observations per imaged area.

We calculated synthetic SWOT observations of river slope, width, and WSE for each modeled pixel as the true model states, plus a measurement error. The true model states were obtained from the true simulation of the LISFLOOD-FP model. For this study, we only considered height measurement error h_{err}. Based on the specification of the SWOT mission, the actual cross-track ground resolution varies from 10 m in the far swath to about 60 m in the near swath. The resolution in the along-track direction is about 2 m, derived by means of synthetic aperture processing. To simplify the model, however, we conservatively assumed that the SWOT spatial resolution in both the along-track and cross-track directions is approximately 50 m. Errors in each SWOT observation were simulated by zero mean Gaussian random error with a standard deviation σ_h of 0.5 m, following previous work (e.g., Durand et al., 2010a; Lee et al., 2010); that is the worst-case of elevation accuracy for SWOT (Enjolras et al., 2006; Rodríguez, 2009). Based on these assumptions, we modeled the measurement error h_{err} using:

$$h_{err} = N\left(0, \frac{1}{\sqrt{n_{obs}}}\sigma_h\right) \tag{7}$$

where n_{obs} is the number of SWOT pixels that would be contained within the LISFLOOD-FP modeled pixel. The n_{obs} is calculated from the river channel width for each LISFLOOD-FP pixel.

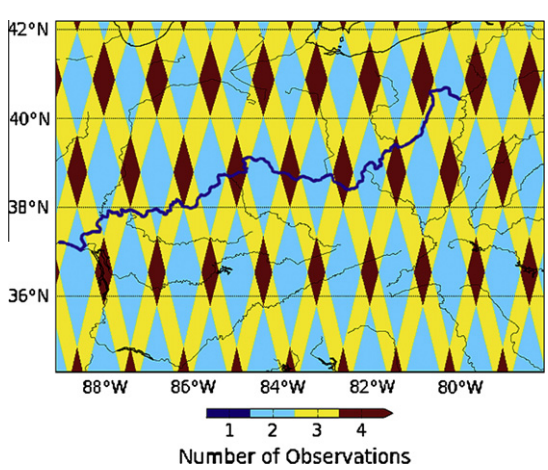

Fig. 5. The number of observations in each SWOT 22-day revisit period. The bold blue curved line is the Ohio River.

5. Data assimilation strategy

5.1. Ensemble Kalman Filter

A data assimilation scheme is typically used to estimate time-varying model state variables, e.g., hydraulic model states, such as discharge or water depth. For example, Andreadis et al. (2007) and Biancamaria et al. (2011) estimated river flow depth using a data assimilation scheme. In addition, data assimilation techniques can be used to estimate model parameters that are not directly observable (e.g., river bathymetry) via state-parameter estimation schemes (Evensen, 2009). In this study we utilize the EnKF

(Evensen, 1994, 2003, 2009) to simultaneously estimate river depth and bathymetry using SWOT observations.

Our implementation of the EnKF algorithm involves: (1) the propagation of the model state variables in time via the LISFLOOD-FP model, and (2) the update of the state variables based on SWOT observations. The EnKF analysis equation for the update is:

$$x_k^+ = x_k^- + K(d + w_k - Hx_k^-) \tag{8}$$

where x^+ is the posterior state estimate (or analysis); x^- is the prior state estimate (or forecast); d is the observation; w is a randomly-generated error included to prevent the introduction of spurious correlations (Burgers et al., 1998); and H is the observation operator, which linearly relates the observations and the state. The Kalman gain, K, is given by:

$$K = P^- H^T (HP^- H^T + R)^{-1} \tag{9}$$

where P^- is the a priori state error covariance that is directly obtained from the ensembles; and R is the observation error covariance that is determined by the uncertainty of the measurements; following previous studies, we assumed measurement errors are uncorrelated, and so that the height error at each pixel can be modeled with Eq. (7); R is thus generated from a multivariate normal distribution with zero mean where the covariance matrix is ${\sigma_h}^2$ on the diagonal, and zero elsewhere.

We apply a data assimilation scheme to simultaneously estimate the river depth y and bathymetry z from measurements of river height d; note $d = z + y$. The vector of unknowns is thus $x = [y,z]$. Thus, at a single location along the river and for a single observation time:

$$Hx = H\begin{bmatrix} y \\ z \end{bmatrix} \tag{10}$$

where $H = [1\ 1]$. To capture the spatial and temporal correlations of the river system, we use a smoothing approach, which is described below.

5.2. Local ensemble batch smoother

River discharge shows a large degree of spatiotemporal autocorrelation; thus, a SWOT measurement at one overpass not only contains information about that time, but also about times prior and after the overpass. An ensemble of model states is sequentially updated through the EnKF when observations become available; thus the method shows the limits of consideration of the spatiotemporal correlation between model states and measurements. Here, we used an ensemble batch smoother (EnBS) algorithm to apply observations made at one overpass to model simulations at other times, and to apply observations of one part of the river to other river locations (Dunne and Entekhabi, 2005). Ensemble smoothers are an extension of the EnKF (Evensen and van Leeuwen, 2000; van Leeuwen and Evensen, 1996). Here, we selected a 22-day smoothing window for batch processing; this was chosen for convenience to correspond to the SWOT repeat cycle. Note that the computational burden increases non-linearly with the length of the smoothing window. The augmented observation vector D contains all observations during the 22-day smoothing window:

$$D = [d_3, d_4, d_6, d_7, d_9, d_{10}, d_{12}, d_{13}, d_{15}, d_{16}, d_{19}, d_{22}]^T \tag{11}$$

where each d_i is a vector of all observed river pixel heights on day i. The subscripts in the above equation refer to the day of the 22-day cycle; some subscripts are absent because no pixel in the model domain was observed on those days. Thus, some part of the Ohio River was observed on 12 of the 22 days of the cycle. The augmented state vector X contains the state of water depths y and bed elevation z at all times, including times when no SWOT observations are available.

$$X = [y_1, y_2, \ldots, y_{22}, z]^T \tag{12}$$

In addition, the covariance matrices P and R were modified to correspond to the augmented observations and state vectors, respectively.

We used localization techniques to avoid spurious correlations between the observations and state variables over long spatial distances (Hamill et al., 2001). In addition, the localization method can be useful to reduce the impact of limited ensemble size (Evensen, 2003, 2009). Here, the covariance localization ρ was used, following Reichle and Koster (2003), utilizing Gaspari and Cohn (1999, their Eq. 4.10). Finally, we used the local ensemble batch smoother (LEnBS) to estimate water depths and the bed elevation from the SWOT observations:

$$X_k^+ = X_k^- + \tilde{K}(D + \tilde{w}_k - HX_k^-) \tag{13}$$

where $\tilde{w}$ is a vector of randomly-generated error, and the Kalman gain $\tilde{K}$ is given by:

$$\tilde{K} = [(\rho \circ \tilde{P})H^T][H(\rho \circ \tilde{P})H^T + \tilde{R}]^{-1} \tag{14}$$

where ρ is the covariance localization; $\tilde{P}$ is a prior state error covariance of the augmented X; $\tilde{R}$ is the observation error covariance of D; $\circ$ is the symbol of the Schur product; and the observation operator H is given by:

$$H = [\,h_1 \quad \ldots \quad h_{22}\,|h_{23}] \tag{15}$$

where h_i is the observation operator of water depth state, which linearly relates the observations d_i to the water depth y_i, for observation day $i = 1,2,\ldots,22$. The operators are diagonal matrices and the diagonal entries contain only 1 and 0; 1 indicates that the state was observed and 0 indicates that it was not. h_{23} is the observation operator of the bed elevation state and is an identity matrix.

6. Experimental design

To evaluate the potential for characterizing the river water depths and bed elevation of the Ohio River from SWOT observations, an OSSE was designed. For the OSSE, synthetic SWOT observations were generated as described in Section 4. Then, we integrated the observations into the LISFLOOD-FP model using the data assimilation scheme described in Section 5 to estimate the bathymetry along the main stem of the Ohio River. The LEnBS scheme is applied sequentially to each 22-day cycle during the experimental period. Uncertainty in bathymetry is sequentially analyzed and updated. There is no feedback to the VIC model for the boundary inflows. We assume that the bathymetry does not change during the simulated period. Given this assumption, the prior state vector X^- of each LEnBS in Eq. (13) was defined by the ensemble generated by an open-loop simulation with the ensemble of boundary inflows for each cycle and the posterior estimate bathymetry of the previous cycle. The study period was March 1, 1996 to 23 August 1996 (176 days or eight SWOT orbit cycles).

The error of the bed elevation and water depth estimates was evaluated after each LEnBS processing cycle by comparison with the true values at each modeled pixel along the main stem of the Ohio River. In addition, we examined how the estimated bathymetry impacted river discharge estimates by determining the difference between true discharges from the LISFLOOD-FP model and estimated instantaneous river discharges at the time of a SWOT measurement. As mentioned above, SWOT can directly measure WSE and surface slope, and channel width can be extracted from the dynamic water mask derived from the SWOT. Thus, the

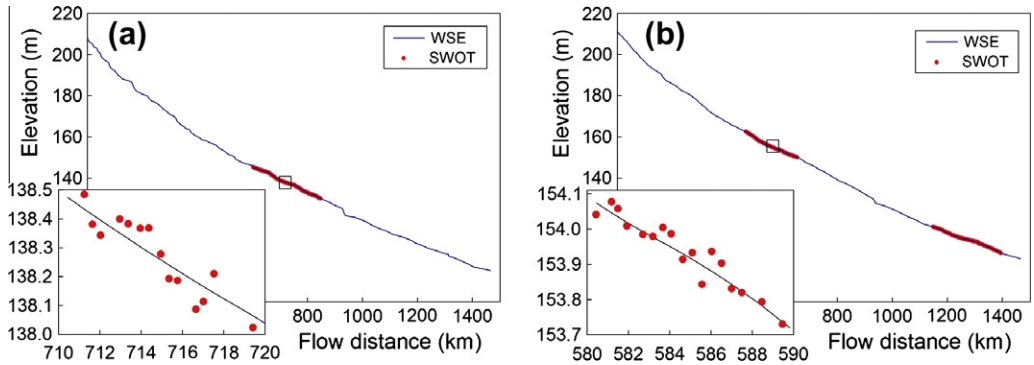

Fig. 6. Graph shows the examples of the synthetic SWOT observations and the WSE simulated by the LISFLOOD-FP for the Ohio River on (a) day 3 and (b) day 16 of the experimental period.

instantaneous river discharges can be calculated using the Manning's equation with SWOT observations and estimated bathymetry from the LEnBS. The equation is given by:

$$\hat{Q}_p^{(t)} = \frac{1}{n_p} w_p y_p^{\frac{5}{3}(t)} S_p^{\frac{1}{2}(t)} \tag{16}$$

where $\hat{Q}_p^{(t)}$ is the estimated discharge at pixel p at every time t; n_p is the Manning's roughness coefficient at pixel p; w_p is the channel width at pixel p (note that roughness and width are assumed to be constant in time); $S_p^{(t)}$ is the surface slope at pixel p at every time t; and channel water depth at pixel p at every time t, $y_p^{(t)}$ is determined by:

$$y_p^{(t)} = d_{p,obs}^{(t)} - \hat{z}_p \tag{17}$$

where $d_{p,obs}^{(t)}$ is the SWOT WSE observation at pixel p at every time t, and $\hat{z}_p$ is the ensemble mean of the bed elevation. The instantaneous discharge error at pixel p, ρ_p, was evaluated by the NRMSE, given by:

$$\rho_p = \frac{\left[\frac{1}{n}\sum_{o=1}^{n_o}\left(Q_{p,est}^{(o)} - Q_{p,true}^{(o)}\right)^2\right]^{0.5}}{\frac{1}{n_t}\sum_{t=1}^{n_t} Q_{p,true}^{(t)}} \tag{18}$$

where n_o is the total number of SWOT observations, and n_t is the total number of days simulated.

7. Results and discussion

7.1. SWOT observations

The Ohio River was measured on days 3, 4, 6, 7, 9, 10, 12, 13, 15, 16, 19, and 22 within the 22-day repeat time (a total of 12 days). Fig. 6 shows examples of the synthetic SWOT WSE observations for the Ohio River main stem derived from the LISFLOOD-FP model results, as described in Section 4. The observed flow distances along the main stem for two different days, day 3 and day 16 of the simulation period, are 259.1 and 459.5 km, respectively, in spite of the 140-km swath of the SWOT. The reason is that the flow direction of the Ohio River is not perpendicular to the satellite track. Some reaches of the Ohio River can be measured twice in a day, depending on the satellite heading direction and the sensor viewing characteristics. All pixels in the Ohio River were measured at least twice in the 22-day cycle and up to four times during the orbital cycle.

7.2. Estimating bed elevation and water depth

Fig. 7 shows the LEnBS assimilation results based on the initial ensemble and the synthetic SWOT observations for the first SWOT cycle, March 1 to March 22. In Fig. 7a, the first-guess of the bed elevation estimates (green[1] dashed line) had a 1.62 m reach-average RMSE. The posterior bed elevation estimates (blue short dashed line) after the assimilation were clearly improved over the prior estimates; the posterior estimates had a 1.30 m reach-average RMSE, which is 19.8% less than the first-guess of the bed elevation estimates. In addition, the posterior estimates clearly follow the spatial pattern of the true bed elevation (red line). There is notable improvement at the Falls of the Ohio, at around the 950 km flow distance. March 12, 1996 was selected for an example of representative river depth estimates and is shown in Fig. 7b. Similar to the bed elevation estimates, the initial prior estimates of water depth showed relatively low correlations of 0.43 when compared

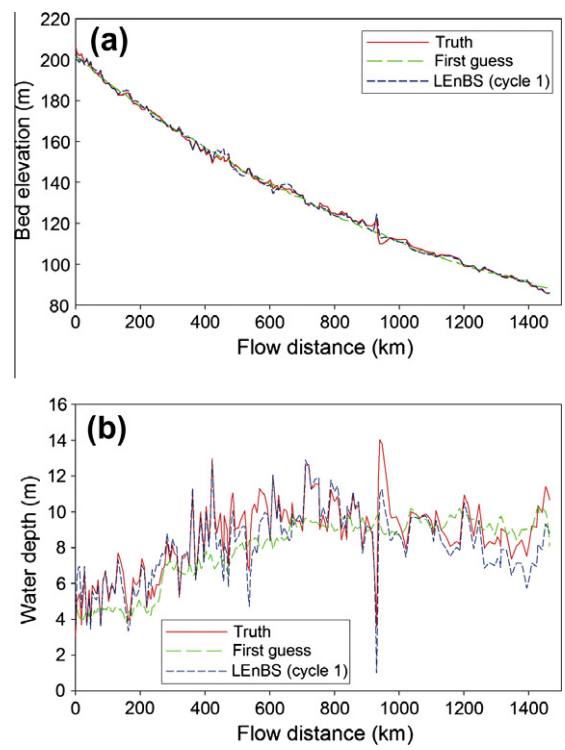

Fig. 7. Examples of the initial estimates of (a) bed elevation and (b) water depth (March 12, 1996). After filtering, the estimates of bed elevation and water depth were clearly improved in both their spatial pattern and accuracy (19.8% and 38.3%, respectively).

[1] For interpretation of color in Figs. 1, 5 and 7, the reader is referred to the web version of this article.

to the truth. After assimilation, the posterior water depth estimates clearly recovered their spatial pattern (correlation coefficient of 0.91), and the reach-average RMSE decreased. The error of the prior estimates is 1.31 m, compared to 0.81 m for the posterior estimates, which is a 38.3% improvement in terms of RMSE.

Fig. 8 presents the mean bed elevation estimates after observation/assimilation cycle 8 along the main stem of the Ohio River, compared with the truth and first-guess simulations. The error after assimilation cycle 8 shows a 0.52 m reach-average RMSE, which is 67.8% less than the first-guess. The first-guess of the bed elevation estimates does not represent the spatial pattern of the Falls (see Fig. 8d). After assimilation, remarkable improvement was observed as more SWOT observations were used.

Fig. 9 shows the reach-average RMSE of each cycle after the LEnBS processing. In general, the errors decreased after performing each LEnBS update. As these bathymetry estimates contain more SWOT observations with additional cycles, the accuracy improves. From the results, however, we also found that the RMSE of the bed elevation estimate increased for cycles 3, 4, and 7.

To explore why bed elevation errors increased during cycles 3, 4, and 7, we divided the main stem of the Ohio River into four sections (Fig. 1; Table 1). In the first section, the Allegheny, Monongahela, Muskingum, and Kanawha Rivers join the main stem of the Ohio River; in the second section, the Big Sandy, Scioto, and Licking Rivers join the main stem; in the third section, the Great Miami and Kentucky Rivers join the main stem; and in the last section, the Green, Wabash, Cumberland, and Tennessee Rivers join the main stem. Fig. 10 shows the reach-average RMSE for the bed elevation of each section (dashed line), compared with the

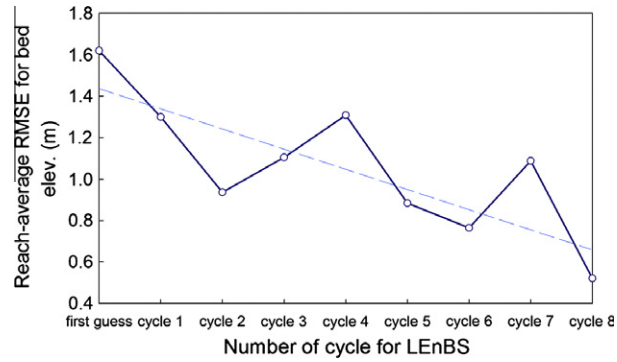

Fig. 9. Graph shows the reach-average RMS error for the bed elevation estimates of each cycle after the LEnBS processing. The error after processing 8 cycles is 0.52 m, a 67.8% improvement in accuracy compared to the first guess bed elevation estimates.

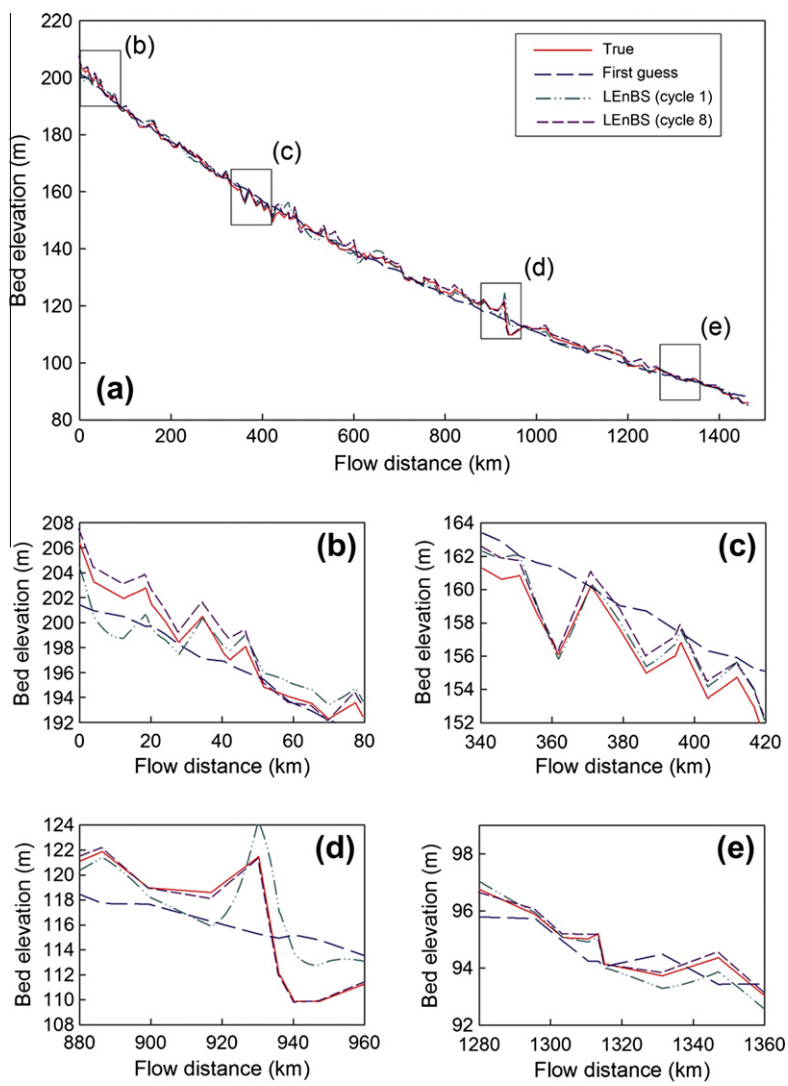

Fig. 8. Graphs show the LEnBS update results (bed elevation) of each cycle. After performing each LEnBS update, the errors were clearly reduced along the Ohio River.

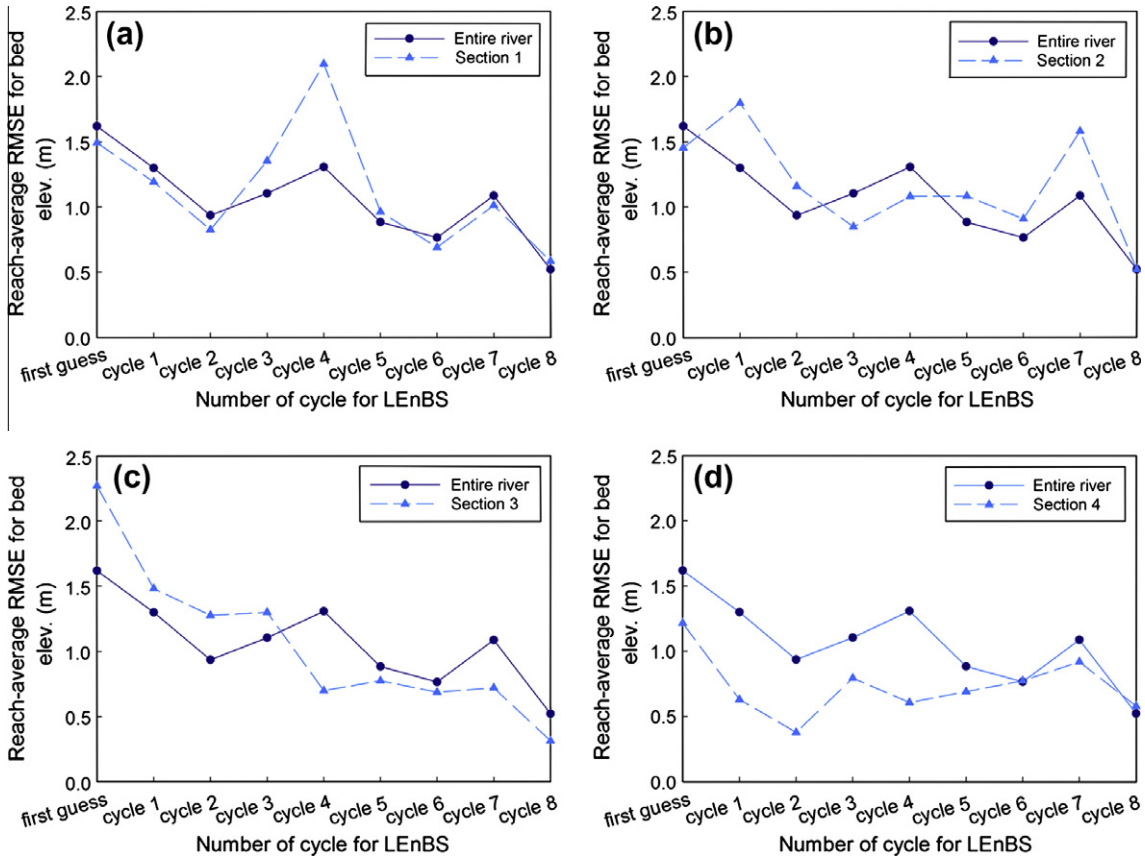

Fig. 10. Graphs show the reach-average RMSE of each section, compared with the RMSE of the entire river after each LEnBS processing cycle.

RMSE of the entire river (solid line) after each LEnBS processing cycle. The increase in error for cycles 3 and 4 mainly came from Section 1 (Fig. 10a) and the increase in error for cycle 7 came from Sections 1 and 2 (Fig. 10a and b). Overall, the accuracy of the upstream sections was not as good as the accuracy of the downstream sections.

The increase in bathymetry errors is due to underestimation of boundary inflows for the upstream river sections during some cycles. Section 1 of the Ohio River has four major and three minor tributaries; hydrographs of these tributaries are shown in Fig. 11. Fig. 11a shows the hydrograph of the gage that corresponds to the Allegheny and Monongahela Rivers, the two rivers that join to form the Ohio River at Pittsburgh, PA. From Fig. 11a, there is a significant underestimation between the true USGS flows and the VIC-generated flow ensemble within the experimental periods of cycles 3 and 4 (45–88 days). Since the assimilation is performed independently for each cycle, there is effectively a severe low bias of the ensemble during cycles 3 and 4. Table 2 shows the RMSE of the discharge and relative bias at the location where each tributary joins the Ohio River main stem. For example, the Allegheny and Monongahela Rivers tributaries had biases of 48.0% and 63.7%, respectively, over cycles 3 and 4 (for details, see Table 2). Significant bias is expected to affect the estimate of the prior water depth. One of the underlying assumptions in the derivation of the EnKF is that the states are unbiased (Evensen, 1994, 2003). If bias is significant, it must be dealt with explicitly within the assimilation scheme; a number of methods exist for doing so (De Lannoy et al., 2007a, 2007b; Keppenne et al., 2005). From Table 2, it appears that approximately 40% bias is a threshold, as shown by the shaded cells. If inflows are less biased than 40%, the LEnBS improved the bathymetry estimates.

7.3. Discharge estimation

Based on first-guess bed elevations and bed elevations estimated by cycles 1 and 8 of the LEnBS, we estimated instantaneous discharge results for the Ohio River at the time of each SWOT overpass over the entire experimental period using Eq. (16). The discharge results were compared to the true values that were modeled by LISFLOOD-FP (for example, see Fig. 12). Fig. 12a and b show the hydrograph at the locations where the Kentucky and Tennessee Rivers join the Ohio River (around 840 and 1450 km flow distance), respectively; the discharge estimates are notably improved by the better bathymetry estimates. The time-averaged discharge RMSE of the entire Ohio River is 1348 m^3/s (35.7% NRMSE) for the first-guess estimates of the bed elevation. The time-averaged discharge RMSEs are 904 m^3/s (27.4% NRMSE) and 389 m^3/s (10.5% NRMSE) with bed elevation estimates at cycles 1 and 8 of the LEnBS, respectively; the errors show a 32.9% and 71.2% improved accuracy compared with the first-guess of the bed elevation, respectively.

The combination of errors in bathymetry and errors in discharge boundary conditions represents a difficult estimation problem, since a discrepancy in the first-guess height and the height observation might be due both to an inaccurate discharge and to inaccurate river bathymetry. The successful estimation of bathymetry illustrates that the assimilation scheme is capable of using the spatial and temporal autocorrelation provided by the hydraulic model to accurately update the first guess of river bathymetry. Essentially, this suggests that the river bathymetry creates a unique water elevation "signature" that is separable from the river discharge signal using the model covariances (see Eq. (14)) and a number of SWOT cycles. In this study, this no longer holds if the

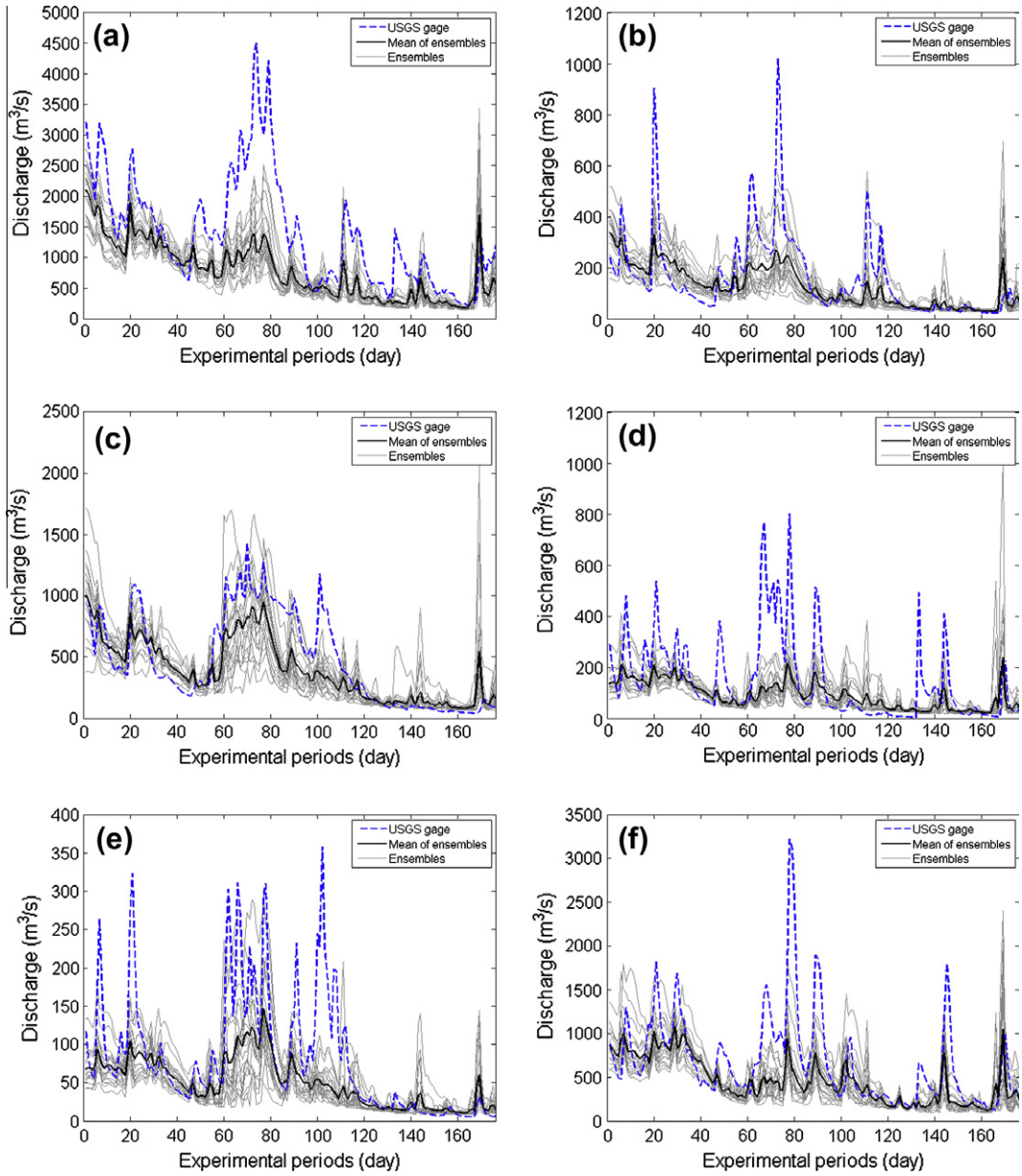

Fig. 11. Hydrographs of six tributaries in Section 1 are shown: (a) Allegheny and Monongahela River, (b) Beaver River, (c) Muskingum River, (d) Little Kanawha River, (e) Hocking River, and (f) Kanawha River.

ensemble is biased more than approximately 40%. Once bathymetry has been estimated, accurate estimates of river discharge can be calculated by using the SWOT observations with the Manning's equation. Future work will explore the effect of errors in Manning's *n*, and the prospects for simultaneous estimation of bathymetry and Manning's *n*.

8. Conclusions

In this study, we presented an algorithm for estimating river bathymetry from the data assimilation of synthetic SWOT observations into the LISFLOOD-FP hydrodynamic model. The LEnBS assimilation framework showed the potential of estimating the bed elevation and water depths from SWOT observations, resulting in improved estimates of river discharge using SWOT observations. Bed elevation was successfully estimated; no in situ measurements of river bathymetry were used in the assimilation framework. We utilized a smoothing window of 22 days, and processed a total of eight 22-day cycles. After the first cycle, the accuracy of the bed elevation estimates was a 1.29 m reach-average RMSE, which is 19.8% less than the first-guess. After cycle 8 (after 176 experimental days), the bathymetry showed a 0.52 m reach-average RMSE, which is 67.8% less than the first-guess. Instantaneous river discharge estimates were computed using Manning's equation, based on bed elevation estimated by the LEnBS. The instantaneous river discharge estimate over the experimental period had a 10.5% NRMSE, which is a 71.2% improved accuracy compared with the river discharge estimates using the first guess of bed elevation.

These results suggest that assimilation processing is useful for estimating river bed elevation. The results also show that large errors in boundary inflows can compromise the accuracy of bed elevation estimates. Accuracy of bed elevation estimates was nonetheless efficiently recovered within the assimilation scheme; the

Table 2
RMSE (m^3/s) of the boundary inflows for each LEnBS processing cycle at the location where each tributary (four major and three minor tributaries) joins the Ohio River in Section 1. The numbers in parenthesis refer to relative bias.

	Upstream of the Ohio River[a]	Beaver River	Muskingum River	Little Kanawha River	Hocking River	Kanawha River
Cycle 1	848.1 (30.4%)	912.1 (27.0%)	990.3 (20.8%)	1,112.9 (21.5%)	1186.7 (33.9%)	1405.9 (32.1%)
Cycle 2	327.0 (24.0%)	301.0 (20.3%)	404.8 (21.0%)	454.1 (21.5%)	467.1 (21.5%)	622.3 (20.6%)
Cycle 3	894.4 (48.0%)	1011.2 (47.2%)	1212.0 (42.6%)	1212.0 (40.2%)	1281.3 (40.3%)	1501.4 (40.1%)
Cycle 4	1995.1 (63.7%)	2184.6 (61.2%)	2487.6 (55.1%)	2724.1 (56.1%)	2777.3 (54.6%)	3683.7 (55.3%)
Cycle 5	428.6 (31.2%)	437.0 (30.3%)	759.8 (38.1%)	806.0 (35.5%)	903.1 (38.1%)	1289.7 (33.5%)
Cycle 6	660.0 (51.6%)	768.7 (49.8%)	809.5 (41.8%)	777.7 (38.7%)	798.7 (38.4%)	824.8 (34.0%)
Cycle 7	532.5 (52.7%)	526.7 (49.2%)	497.0 (38.6%)	613.8 (40.8%)	616.6 (40.0%)	1028.2 (43.7%)
Cycle 8	328.5 (35.3%)	360.3 (32.9%)	427.8 (25.3%)	447.8 (26.9%)	452.7 (26.5%)	573.2 (30.4%)

[a] These boundary inflows include the Allegheny and Monongahela River drainage basins.

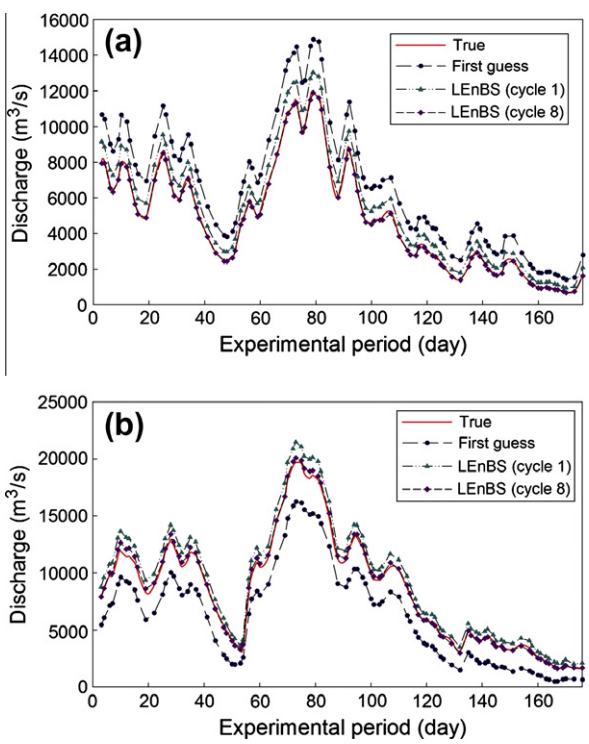

Fig. 12. Instantaneous discharge results corresponding to bathymetry estimates of first-guess, cycles 1 and 8 of LEnBS over the entire experimental period are shown as point, triangle, and diamond, respectively; the hydrograph at the locations where the (a) Kentucky and (b) Tennessee Rivers join into the Ohio River (around 840- and 1450-km flow distance), respectively.

assimilation scheme tended to degrade the bathymetry estimates for cycles where the boundary inflows were biased more than 40%.

In this study, we only considered two critical uncertainties: precipitation forcing that propagates to boundary inflows and river bathymetry errors. Future work will consider other uncertainties in the model, such as the Manning's roughness coefficient, as well as generating more realistic SWOT observations, including effects such as layover. In addition, a bias correction method needs to be considered to improve the accuracy of the estimates.

Acknowledgments

This work was partially supported by The Ohio State University Climate, Water and Carbon program, NASA Physical Oceanography Grant NNX10AE96G, and NASA Headquarters under the NASA Earth and Space Science Fellowship Program-Grant NNX11AL60H. The authors would like to thank Trent Schade and Deborah Lee at the U.S. Army Corps of Engineers, Ohio River Division, Cincinnati, Ohio for the bathymetric data of the Ohio River. Computational support for this project was provided by the Ohio Supercomputer Center, under Project PAS0503.

References

Alsdorf, D.E., Rodriguez, E., Lettenmaier, D.P., 2007a. Measuring surface water from space. Rev. Geophys. 45 (2).
Alsdorf, D., Bates, P., Melack, J., Wilson, M., Dunne, T., 2007b. Spatial and temporal complexity of the Amazon flood measured from space. Geophys. Res. Lett. 34, L08402.
Andreadis, K.M., Clark, E.A., Lettenmaier, D.P., Alsdorf, D.E., 2007. Prospects for river discharge and depth estimation through assimilation of swath-altimetry into a raster-based hydrodynamics model. Geophys. Res. Lett. 34, L10403.
Bates, P.D., De Roo, A.P.J., 2000. A simple raster-based model for flood inundation simulation. J. Hydrol. 236, 54–77.
Benke, A., Cushing, C., 2005. Rivers of North America. Elsevier Academic Press, pp. 375–424.
Biancamaria, S., Durand, M., Andreadis, K.M., Bates, P.D., Boone, A., Mognard, N.M., Rodríguez, E., Alsdorf, D.E., Lettenmaier, D.P., Clark, E.A., 2011. Assimilation of virtual wide swath altimetry to improve Arctic river modeling. Remote Sens. Environ. 115, 373–381.
Bjerklie, D.M., Moller, D., Smith, L.C., Dingman, S.L., 2005. Estimating discharge in rivers using remotely sensed hydraulic information. J. Hydrol. 309 (2005), 191–209.
Bowling, L.C., Lettenmaier, D.P., 2010. Modeling the effects of lakes and wetlands on the water balance of Arctic environments. J. Hydrometeorol. 11, 276–295.
Brackenridge, G.R., Nghiem, S.V., Anderson, E., Chien, S., 2005. Space-based measurement of river runoff. EOS 86 (19), 185–188.
Burgers, G., van Leeuwen, P.J., Evensen, G., 1998. Analysis scheme in the ensemble Kalman filter. Mon. Weather Rev. 126, 1719–1724.
Chow, V.T., 1959. Open-Channel Hydraulics. McGraw-Hill, New York.
De Lannoy, G.J.M., Houser, P.R., Pauwels, V.R.N., Verhoest, N.E.C., 2007a. State and bias estimation for soil moisture profiles by an ensemble Kalman filter: effect of assimilation depth and frequency. Water Resour. Res. 43, W06401.
De Lannoy, G.J.M., Reichle, R.H., Houser, P.R., Pauwels, V.R.N., Verhoest, N.E.C., 2007b. Correcting for forecast bias in soil moisture assimilation with the ensemble Kalman filter. Water Resour. Res. 43, W09410.
Dunne, S., Entekhabi, D., 2005. An ensemble-based reanalysis approach to land data assimilation. Water Resour. Res. 41, W02013.
Durand, M., Andreadis, K.M., Alsdorf, D.E., Lettenmaier, D.P., Moller, D., Wilson, M., 2008. Estimation of bathymetric depth and slope from data assimilation of swath altimetry into a hydrodynamic model. Geophys. Res. Lett. 35, L20401.

Durand, M., Rodríguez, E., Alsdorf, D.E., Trigg, E., 2010a. Estimating river depth from remote sensing swath interferometry measurements of river height, slope, and width. IEEE J. Sel. Topics Appl. Earth Observat. Remote Sens. 3 (1), 20–31.
Durand, M., Fu, L., Lettenmaier, D.P., Alsdorf, D.E., Rodríguez, E., Esteban-Fernandez, D., 2010b. The surface water and ocean topography mission: observing terrestrial surface water and oceanic submesoscale eddies. Proc. IEEE 98 (5), 766–779.
Enjolras, V., Vincent, P., Souyris, J.-C., Rodríguez, E., Phalippou, L., Cazenave, A., 2006. Performances study of interferometric radar altimeters: from the instrument to the global mission definition. Sensors 6, 164–192.
Evensen, G., 1994. Sequential data assimilation with a nonlinear quasi-geostrophic model using Monte-Carlo methods to forecast error statistics. J. Geophys. Res. 99 (C5), 10143–10162.
Evensen, G., van Leeuwen, P.J., 2000. An ensemble Kalman smoother for nonlinear dynamics. Mon. Weather Rev. 128 (6), 1852–1867.
Evensen, G., 2003. The ensemble Kalman filter: theoretical formulation and practical implementation. Ocean Dynam. 53, 343–367.
Evensen, G., 2009. The ensemble Kalman filter for combined state and parameter estimation. IEEE Control. Syst. Mag. 29 (3), 82–104.
Fonstad, M., Marcus, W., 2005. Remote sensing of stream depths with hydraulically assisted bathymetry (HAB) models. Geomorphology 72 (1–4), 320–339.
Furey, P.R., Gupta, V.K., 2005. Effects of excess rainfall on the temporal variability of observed peak-discharge power laws. Adv. Water Resour. 28, 1240–1253.
Gaspari, G., Cohn, S.E., 1999. Construction of correlation functions in two and three dimensions. Quart. J. R. Meteorol. Soc. 125 (554), 723–757.
Giustarini, L., Matgen, P., Hostache, R., Montanari, M., Plaza, D., Pauwels, V.R.N., De Lannoy, G.J.M., De Keyser, R., Pfister, L., Hoffmann, L., Savenije, H.H.G., 2011. Assimilating SAR-derived water level data into a flood model: a case study. Hydrol. Earth Syst. Sc. 15, 2349–2365.
Hamill, T.M., Whitaker, J.S., Snyder, C., 2001. Distance-dependent filtering of background error covariance estimates in an ensemble Kalman filter. Mon. Weather Rev. 129 (11), 2776–2790.
Hostache, R., Matgen, P., Schumann, G., Puech, C., Hoffmann, L., Pfister, L., 2009. Water level estimation and reduction of hydraulic model calibration uncertainties using satellite SAR images of floods. IEEE Trans. Geosci. Remote Sens. 47, 431–441.
Hunter, N.M., Bates, P.D., Neelz, S., Pender, G., Villanueva, I., Wright, N.G., Liang, D., Falconer, R.A., Lin, B., Waller, S., Crossley, A.J., Mason, D.C., 2008. Benchmarking 2D hydraulic models for urban flooding. Proc. ICE – Water Manage. 161 (1), 13–30.
Keppenne, L.C., Rienecker, M.M., Kurkowski, N.P., Adamec, D.A., 2005. Ensemble Kalman filter assimilation of temperature and altimeter data with bias correction and application to seasonal prediction. Non-linear Process. Geophys. 12, 491–503.
Kouraev, A.V., Zakharova, E.A., Samain, O., Mognard, N.M., Cazenave, A., 2004. Ob' river discharge from TOPEX/Poseidon satellite altimetry (1992–2002). Remote Sens. Environ. 93 (1–2), 238–245.
Lafon, V., Froidefond, J.M., Lahet, F., Castaing, P., 2002. SPOT shallow water bathymetry of a moderately turbid inlet based on field measurements. Remote Sens. Environ. 81 (1), 136–148.
Lee, D.H., Wisbith, S.M., McKee, G.M., Jackson, H.C., Buelow, D.P., 2003. Modeling and Managing the Ohio River. USACE Informal Technical Report.
Lee, H., Durand, M., Jung, H.C., Alsdorf, D., Shum, C.K., Sheng, Y., 2010. Characterization of surface water storage changes in Arctic lakes using simulated SWOT measurements. Int. J. Remote Sens. 31 (14), 3931–3953.
LeFavour, G., Alsdorf, D., 2005. Water slope and discharge in the Amazon River estimated using the shuttle radar topography mission digital elevation model. Geophys. Res. Lett. 32, L17404.
Liang, X., Lettenmaier, D.P., Wood, E.F., Burges, S.J., 1994. A simple hydrologically based model of land surface water and energy fluxes for GSMs. J. Geophys. Res. 99 (D7), 14415–14428.
Liang, X., Wood, E.F., Lettenmaier, D.P., 1996. Surface soil moisture parameterization of the VIC-2L model: evaluation and modifications. Global Planet. Change 13, 195–206.
Lowrey, M.R.K., Yang, Z.L., 2008. Assessing the capability of a regional-scale weather model to simulate extreme precipitation patterns and flooding in central Texas. Weather. Forecast. 23 (6), 1102–1126.
Matgen, P., Montanari, M., Hostache, R., Pfister, L., Hoffmann, L., Plaza, D., Pauwels, V.R.N., De Lannoy, G.J.M., De Keyser, R., Savenije, H.H.G., 2010. Towards the sequential assimilation of SAR-derived water stages into hydraulic models using the particle filter: proof of concept. Hydrol. Earth Syst. Sci. 14, 1773–1785.
Maurer, E.P., Wood, A.E., Adam, J.C., Lettenmaier, D.P., 2002. A long-term hydrologically based dataset of land surface fluxes and states for the conterminous United States. J. Climate. 15, 3237–3251.
Neal, J.C., Schumann, G., Bates, P.D., Buytaert, W., Matgen, P., Pappenberger, F., 2009. A data assimilation approach to discharge from space. Hydrol. Process. 23, 3641–3649.
Neal, J.C., Schumann, G., Fewtrell, T., Budimir, M., Bates, P., Mason, D., 2011. Evaluating a new LISFLOOD-FP formulation with data from the summer 2007 floods in Tewkesbury, UK. J. Flood Risk Manage. 4 (2), 88–95.
Nijssen, B., Lettenmaier, D.P., 2004. Effect of precipitation sampling error on simulated hydrological fluxes and states: anticipating the global precipitation measurement satellites. J. Geophys. Res. 109, D02103.
Pavelsky, T., Smith, L.C., 2008. RivWidth: a software tool for calculation of river widths from remotely sensed imagery. IEEE Geosci. Remote Sens. Lett. 5 (1), 70–73.
Reichle, R.H., Koster, R.D., 2003. Assessing the impact of horizontal error correlations in background fields on soil moisture estimation. J. Hydrometeor. 4, 1229–1242.
Reichle, R.H., 2008. Data assimilation methods in the earth sciences. Adv. Water Resour. 31, 1411–1418.
Rodríguez, E., 2009. SWOT Science Requirements Document. JPL Document, Initial Release. <http://swot.jpl.nasa.gov/files/SWOT_science_reqs_final.pdf>.
Schumann, G., Di Baldassarre, G., Alsdorf, D., Bates, P.D., 2010. Near real time flood wave approximation on large rivers from space: application to the River Po, Italy. Water Resour. Res. 46, W05601.
Trigg, M.A., Wilson, M.D., Bates, P.D., Horritt, M.S., Alsdorf, D.E., Forsberg, B.R., Vega, M.C., 2009. Amazon flood wave hydraulics. J. Hydrol. 374, 92–1015.
van Leeuwen, P.J., Evensen, G., 1996. Data assimilation and inverse methods in terms of a probabilistic formulation. Mon. Weather Rev. 124, 2898–2913.
Zhang, Y., Geo, J., Gu, Y., 2011. A simple method for mapping bathymetry over turbid coastal waters from MODIS data: possibilities and limitations. Int. J. Remote Sens. 32 (22), 7575–7590.
Zwenzner, H., Voigt, S., 2009. Improved estimation of flood parameters by combining space based SAR data with very high resolution digital elevation data. Hydrol. Earth Syst. Sci. 13, 567–576.